Supplementary Material for "Thin-Liquid-Film Flow on Three-Dimensional Topographically Patterned Rotating Cylinders"

Chance Parrish, Lucas Pham, and Satish Kumar[1]

Department of Chemical Engineering and Materials Science, University of Minnesota, Minneapolis, MN 55455, USA

In this supplementary material, we describe the linear stability analysis carried out to investigate the growth of the Rayleigh-Plateau-like (RP) instability on angularly patterned cylinders. When the cylinder rotates so rapidly that gravity may be neglected, a gravitational timescale is no longer appropriate. The evolution equation for the film thickness (main text Eqn. (2.18)) may be rescaled using a capillary timescale to yield

$$(1+\epsilon h+\epsilon B)\,\frac{\partial h}{\partial t}=-\epsilon^3\widetilde{\boldsymbol{\nabla}}\cdot\left(\frac{h^3}{3}\left[We\widetilde{\boldsymbol{\nabla}}(h+B)+\widetilde{\boldsymbol{\nabla}}\left(h+B+\widetilde{\nabla}^2(h+B)\right)\right]\right), \tag{0.1}$$

where Eqn. (0.1) was provided as Eqn. (3.1) in the main text. When the topography $B=0$, Eqn. (0.1) reduces to the evolution equation in the limit of a rapidly rotating cylinder found in Evans *et al.* (2005).

1. Linear stability analysis

A linear stability analysis (LSA) may be used to examine the growth of small-amplitude disturbances in the coating thickness on rapidly rotating, topographically patterned cylinders. As a continuous function for the topography $B(\theta,z)$ may be represented by a Fourier series, we carry out the LSA using a screw-shaped topography for simplicity,

$$B(\theta,z)=\beta\cos\left(k_\theta\theta+k_z z\right), \tag{1.1}$$

where β is the amplitude of the topography, and k_θ and k_z are wavenumbers of the topography in the axial and angular directions, respectively. We note that Eqn. (1.1) comprises an even Fourier mode (cosines) and that the LSA will yield a similar result for odd Fourier modes (sines). Due to periodicity of the topography in the θ-direction, k_θ is restricted to integer values.

[1]Email address for correspondence: kumar030@umn.edu

The film thickness is then decomposed into a base state $h_b = 1$ disturbed by a sinusoidal disturbance of an initially small amplitude α with a time-dependent amplitude of $\alpha\overline{h}(t)$,

$$h(\theta, t) = 1 + \alpha\overline{h}(t)\cos\left(l_\theta\theta + l_z z\right) + \mathcal{O}\left(\alpha^2\right). \tag{1.2}$$

The frozen-base-state assumption has been invoked, where the base state h_b is assumed to evolve slowly compared to the disturbance. The wavenumbers of the disturbance l_θ and l_z do not need to be identical to the topography wavenumber. We assume that the topography amplitude β is of $\mathcal{O}(\alpha)$ for the purposes of the LSA.

A non-autonomous ordinary differential equation describing $\overline{h}(t)$ may be obtained after substituting Eqns. (1.1) and (1.2) into Eqn. (0.1) and linearizing with respect to α,

$$\frac{\partial\overline{h}(t)}{\partial t} = \overline{h}(t)\frac{\epsilon^3}{3(1+\epsilon)}\left((1+We)l^2 - l^4\right) + \delta_{k_\theta l_\theta}\delta_{k_z l_z}\frac{\beta}{\alpha}\frac{\epsilon^3}{3(1+\epsilon)}\left((1+We)l^2 - l^4\right), \tag{1.3}$$

where δ_{ij} is the Kronecker delta. The lumped wavenumber l is expressed as $l^2 = l_\theta^2 + l_z^2$. The product of the two Kronecker deltas results from the inner product of the disturbance and the topography,

$$\delta_{k_\theta l_\theta}\delta_{k_z l_z} = \int_0^{2\pi}\int_0^{2\pi}\cos\left(k_\theta\theta + k_z z\right)\cos\left(l_\theta\theta + l_z z\right)d\theta dz, \tag{1.4}$$

and is zero when these Fourier modes are orthogonal ($k_\theta \neq l_\theta$ or $k_z \neq l_z$). Eqn. (1.3) is solved using the integrating-factor method to yield

$$\overline{h}(t) = e^{\omega t} + \delta_{k_\theta l_\theta}\delta_{k_z l_z}\frac{\beta}{\alpha}\left(e^{\omega t} - 1\right), \tag{1.5}$$

where ω is a growth rate given by

$$\omega = \frac{\epsilon^3}{3(1+\epsilon)}\left((1+We)l^2 - l^4\right), \tag{1.6}$$

and β/α is the ratio of the topography amplitude to the disturbance amplitude. The first term on the right-hand side of Eqn. (1.5) describes the effects of centrifugal and capillary forces on the coating in the absence of topography ($\beta = 0$), while the second term captures centrifugal and capillary effects induced by the topography. For an unpatterned cylinder ($\beta = 0$) or a disturbance orthogonal to the topography ($\delta_{k_\theta l_\theta} = 0$ or $\delta_{k_z l_z} = 0$), the results of the LSA reduce to those obtained in Evans *et al.* (2005).

When the topography interacts with the disturbance ($\delta_{k_\theta l_\theta} \neq 0$ and $\delta_{k_z l_z} \neq 0$), the behavior of the coating is controlled by the sign of ω and the ratio of the topography amplitude to the disturbance amplitude (β/α). Centrifugal forces dominate when $\omega > 0$, causing liquid to accumulate over pattern crests ($\overline{h}(t) > 0$). Surface-tension forces dominate when $\omega < 0$, causing liquid to accumulate in pattern troughs ($\overline{h}(t) < 0$). When $\omega < 0$, Eqn. (1.5) predicts that the disturbance amplitude should decay exponentially toward $-\beta/\alpha$. For a fixed wavenumbers l_θ and l_z, the critical Weber number separating these regimes ($\omega(We) = 0$) can be found using Eqn. (3.13) in the main text, provided again below,

$$We_c = l_\theta^2 + l_z^2 - 1. \tag{1.7}$$

To examine the effects of ω and of β/α on the evolution of disturbances, simulations of Eqn. (0.1) have been carried out with an initial thickness

$$h_0 = h_b + \alpha \cos\left(l_\theta \theta + l_z z\right), \tag{1.8}$$

on an axially-patterned cylinder ($k_\theta = 0$ and $k_z = 3$). The amplitude $\overline{h}(t)$ is calculated from simulation results by solving Eqn. (1.2),

$$\overline{h}(t) = \frac{h(\theta_0, z_0, t) - 1}{\alpha \cos\left(l_\theta \theta_0 + l_z z_0\right)}, \tag{1.9}$$

where $h(\theta_0, z_0, t)$ is the film thickness obtained from simulations at a fixed angular coordinate θ_0 and axial coordinate z_0. The coating is disturbed by a sinusoidal disturbance (Eqn. (1.2)) of wavenumbers $l_\theta = 0$ and $l_z = 3$ with an initial amplitude of $\alpha = 1 \times 10^{-3}$. The sign of the growth rate ω is varied by changing the Weber number We.

Disturbance amplitudes calculated from simulations (Eqn. (1.9)) on axially patterned cylinders ($k_\theta = 0$ and $k_z = 3$) are compared to the value predicted by the LSA (Eqn. (1.5)) over time for varying ω and varying amplitude ratios β/α in Fig. 1. Solid symbols represent the results calculated from simulations (Eqn. (1.9)) while the solid lines are the results predicted using Eqn. (1.5). The dashed line denoting $\overline{h}(t) = 1$ visually separates results for $\omega > 0$, which fall above the dashed line, and $\omega < 0$, which fall below the dashed line. Arrows mark the direction of increasing β/α.

Good agreement is observed between the disturbance amplitudes calculated from simulations

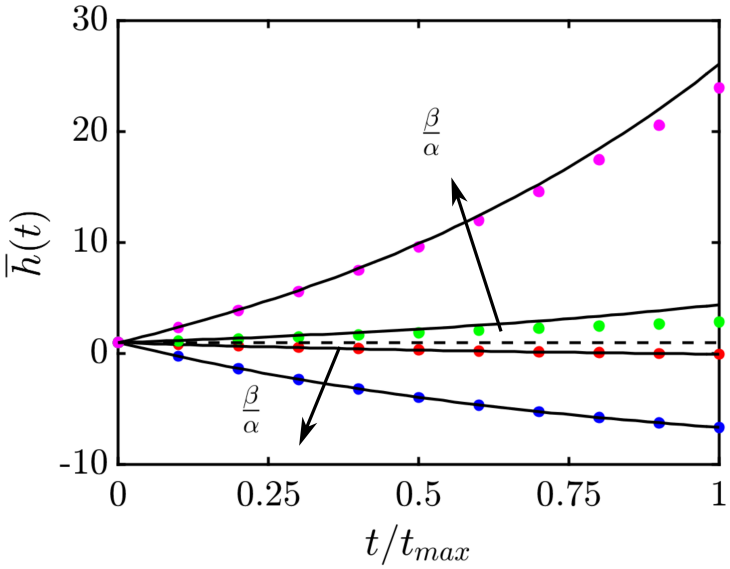

FIG. 1. Simulation results (filled symbols) and LSA predictions (solid lines) for the disturbance amplitude $\overline{h}(t)$. The growth rates are $\omega = \pm 2.667 \times 10^{-5}$ for $We = 20$ and $We = 10$, respectively. Initial disturbance amplitudes were fixed at $\alpha = 1 \times 10^{-3}$ with amplitude ratios β/α of 1 and 10. A horizontal dashed line marks $\overline{h}(t) = 1$—results for $We > We_c$ and $We < We_c$ are found above and below this dashed line, respectively. Arrows mark the direction of increasing β/α.

(symbols) and predicted from the LSA (solid lines), as shown in Fig. 1. For both $\omega > 0$ and $\omega < 0$, an increase in β/α speeds up the evolution of the disturbance as $\overline{h}(t)$ is larger at earlier times (Eqn. (1.5)). At later times in the simulations for $\omega > 0$, the disturbances have grown large enough so that nonlinear effects begin to slow their growth, leading to amplitudes smaller than those predicted by LSA. At times later than those shown in Fig. 1, the disturbance amplitudes with $\omega < 0$ decay exponentially toward $-\beta/\alpha$ as is predicted by Eqn. (1.5). When $l_z \neq k_z$ or $l_\theta \neq k_\theta$, the LSA results reduce to those obtained on an unpatterned cylinder (Eqn. (1.5)) where growth or decay of disturbances is controlled by the sign and magnitude of the growth rate. The growth or decay of these disturbances ($l_z \neq k_z$ or $l_\theta \neq k_\theta$) may compete with the pooling of liquid over crests or troughs induced by the topography ($l_z = k_z$ and $l_\theta = k_\theta$), and evolution of the coating may depend on nonlinear effects that become important at later times.

2. RP wavelength on angularly patterned cylinders

An example of a disturbance orthogonal to the topography ($k_\theta \neq l_\theta$ and/or $k_z \neq l_z$) is an axial disturbance ($l_\theta = 0$ and $l_z \neq 0$) on an angularly patterned cylinder ($k_\theta \neq 0$ and $k_z = 0$). For short times where linearization is valid, disturbances will either grow or decay based on their proximity

to the cutoff wavenumber l_c, where $\omega(k) = 0$ (see Eqn. (1.6),

$$l_c = \sqrt{l_{\theta,c}^2 + l_{z,c}^2} = \sqrt{We + 1}. \tag{2.1}$$

Disturbances with $l > l_c$ will grow due to centrifugal forces while those with $l < l_c$ will be leveled by surface-tension forces. Furthermore, the fastest-growing wavenumbers $l_{\theta,m}$ and $l_{z,m}$ are the wavenumbers at which the growth rate ω is maximized,

$$l_{\theta,m}^2 + l_{z,m}^2 = \frac{We + 1}{2}. \tag{2.2}$$

Due to periodicity in the θ direction, $l_{\theta,m}$ is restricted to the closest integer wavenumber with the largest growth rate (Eqn. (1.6)). The wavelengths of the fastest-growing disturbances with wavenumbers $l_{\theta,m}$ and $l_{z,m}$ are

$$\lambda_{i,m} = \frac{2\pi}{l_{i,m}} \qquad (i = \theta, z)\,. \tag{2.3}$$

For short times in simulations when the linearization of Eqn. (0.1) is valid, the spacings between droplets observed in the θ and z directions are expected to be the wavelengths of the fastest-growing disturbances.

In Evans *et al.* (2005) and Li & Kumar (2018), the dimensionless spacing between rings that form on rapidly rotating, unpatterned cylinders was assumed to be equal to the wavelength of the fastest-growing axial disturbance when angular thickness variations were neglected. On an angularly patterned cylinder, the growth of axial disturbances is predicted to occur independent of the angular patterning by the LSA results (Eqn. (1.5) for $k_z = 0 \neq l_z$). After assuming angular thickness variations are negligible ($l_{\theta,m} = 0$ in Eqn. (2.2)) (Evans *et al.*, 2005; Li & Kumar, 2018), the expression for the dimensionless wavelength of the Rayleigh-Plateau-like (RP) disturbance λ_{RP}^* on an angularly patterned cylinder is obtained from Eqns. (2.2) and (2.3),

$$\lambda_{RP}^* = \frac{2\pi\sqrt{2}}{\sqrt{1 + We}}. \tag{2.4}$$

This expression, also shown in the main text as Eqn. (3.2), is identical to the expression for the dimensionless wavelength of the RP disturbance on unpatterned cylinders. The growth rate ω_m of the disturbance with the wavelength given in Eqn. (2.4) is found by evaluating Eqn. (1.6) for $l_\theta = 0$

and $l_z = \sqrt{0.5\,(1+We)}$,

$$\omega_m = \frac{\epsilon^3\,(1+We)^2}{12\,(1+\epsilon)}. \tag{2.5}$$

This is provided in the main text as Eqn. (3.3).

References

EVANS, P. L., SCHWARTZ, L. W. & ROY, R. V. 2005 Three-dimensional solutions for coating flow on a rotating horizontal cylinder: Theory and experiment. *Phys. Fluids* **17** (7), 072102.

LI, W. & KUMAR, S. 2018 Three-dimensional surfactant-covered flows of thin liquid films on rotating cylinders. *J. Fluid Mech.* **844**, 61–91.